

Uncertainty-Aware Critic Augmentation for Hierarchical Multi-Agent EV Charging Control

Lo Pang-Yun Ting^{1,2,*}, Ali Şenol², Huan-Yang Wang¹, Hsu-Chao Lai¹,
Kun-Ta Chuang¹, Huan Liu²

¹ Dept. of Computer Science and Information Engineering, National Cheng Kung University, Taiwan

Emails: {lpyting, hywang, hclai}@netdb.csie.ncku.edu.tw, ktchuang@mail.ncku.edu.tw

² School of Computing and Augmented Intelligence, Arizona State University, USA

Emails: {lting5, asenol, huanliu}@asu.edu

Abstract

The advanced bidirectional EV charging and discharging technology, aimed at supporting grid stability and emergency operations, has driven a growing interest in workplace applications. It not only reduces electricity expenses but also enhances the resilience in handling practical matters, such as peak power limitation, fluctuating energy prices, and unpredictable EV departures. Considering these factors systematically can benefit energy efficiency in office buildings and for EV users simultaneously. To employ AI to address these issues, we propose *HUCA*, a novel real-time charging control for regulating energy demands for both the building and EVs. *HUCA* employs hierarchical actor-critic networks to dynamically reduce electricity costs in buildings, accounting for the needs of EV charging in the dynamic pricing scenario. To tackle the uncertain EV departures, we introduce a new critic augmentation to account for departure uncertainties in evaluating the charging decisions, while maintaining the robustness of the charging control. Experiments on real-world electricity datasets under both simulated *certain and uncertain departure scenarios* demonstrate that *HUCA* outperforms baselines in terms of total electricity costs while maintaining competitive performance in fulfilling EV charging requirements. A case study also manifests that *HUCA* effectively balances energy supply between the building and EVs based on real-time information, showcasing its potential as a key AI-driven solution for vehicle charging control.

keywords: Hierarchical reinforcement learning, EV bidirectional charging, real-time charging control, dynamic pricing

*Work done during Lo Pang-Yun Ting being a visiting scholar at Arizona State University.

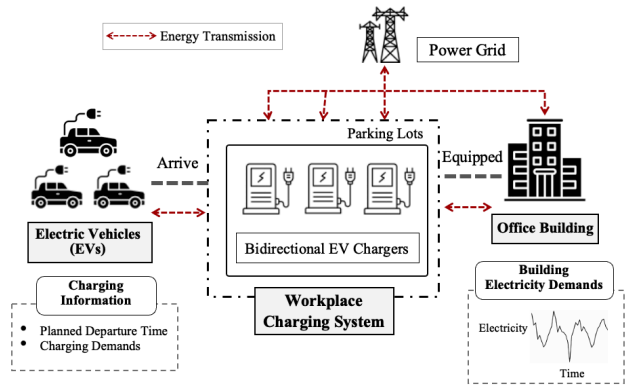


Figure 1: The illustration of the workplace charging scenario with the bidirectional EV chargers.

1 Introduction

Background. The rapid growth in Electric Vehicle (EV) adoption, driven by global sustainability efforts, has led to a surge in demand for advanced charging solutions. According to a report by CBRE Group (Coldwell Banker Richard Ellis Group) Incorporated [4], workplace charging sessions increased at twice the rate of new charging station installations in 2023. This highlights the growing interest for EV charging options in the workplace. Meanwhile, recent advances in *bidirectional charging systems* [19] [24], which support both Grid-to-Vehicle (G2V) and Vehicle-to-Grid (V2G) power flows, have shown the potential to enhance flexibility with regard to charging stability and emergency situations. The effectiveness of bidirectional charging systems has inspired us to explore how better scheduling of G2V and V2G timings can balance the demand for EV charging and reduce overall electricity costs.

In particular, EVs often remain stationary for long periods at office locations, as expected. This prolonged parking time allows for more flexible charging strategies, enabling energy transfer between EVs and office

building. An example of a workplace charging system is shown in Figure 1. Upon arrival, each EV is coordinated by the charging system, with users first providing information such as their charging requirements and anticipated departure time. With such information, the system decides whether to discharge energy from the EV to the building (using V2G) during high-price periods or to charge the EV from the grid to meet its demand before departure (using G2V). Either the V2G or the G2V option can be determined on-the-fly according to the optimal decision-making criteria.

Challenges. For real-time charging control of EVs in various scenarios, previous studies [20] [6] have explored the use of multi-agent reinforcement learning (MARL) techniques to regulate EV charging and discharging actions. However, most existing approaches fail to consider real-world *dynamic factors*, such as dynamic energy prices and the possibility that EV users may depart earlier than the expected time, which complicate determining optimal control strategies for each EV. Moreover, to avert transformer overloads that could destabilize the power grid [25], it is necessary to impose *charging power limits*, thereby further complicating the management of EV charging. These dynamics and limitations pose significant challenges in balancing the energy supply between the building and EVs while minimizing electricity costs. It is crucial to recognize that managing charging improperly could result in considerably higher electricity bills, as power companies will levy extra charges due to overconsumption of energy [18].

Proposed Method. To tackle these challenges, we propose *HUCA* (**H**ierarchical **M**ulti-Agent **C**ontrol with **U**ncertainty-Aware **C**ritic **A**ugmentation), a novel framework designed for real-time charging control. *HUCA* operates under dynamic pricing and penalty mechanisms, consistent with practical situations. A new hierarchical multi-agent framework is devised to balance the energy supply between the building and EVs in dynamic and uncertain environments. The *HUCA* framework consists of two levels of control: a high-level agent and multiple low-level agents. The **high-level agent** determines whether to charge or discharge EVs, which is a collective decision for all EVs. Based on the high-level decision, the **low-level agents** collaboratively and dynamically modulate the individual charging (or discharging) power level for each EV, ensuring they stay within the specified charging power limits, with the goal of satisfying anticipated demands and avoiding transformer overload.

A key innovation of *HUCA* lies in its capability to handle EVs that deviate from their expected departure times. These unpredictable departures introduce uncertainty, potentially disrupting low-level agents’ charging

decisions. To address this, we propose an **uncertainty-aware critic augmentation** mechanism, which assesses the likelihood of departure deviation and adjusts the assessments of low-level agents’ charging decisions accordingly. This mechanism achieves two objectives: **(i)** accounting for uncertainties into the assessment of low-level agents’ decisions, and **(ii)** limiting the direct effect of uncertainties to the present time slot, ensuring the robustness of future decision assessments. Therefore, *HUCA* dynamically adapts to arbitrary EV behaviors while maintaining robust charging control. *HUCA* is designed to minimize the electricity costs of the building while striving to fulfill EV charging demands in a dynamic environment.

The main contributions in this paper are as follows:

- **Real-Time Charging Control:** We propose *HUCA*, a novel hierarchical multi-agent structure that balances energy supply between the building and EVs, which optimizes charging controls on-the-fly.
- **Uncertainties and Limitations Handling:** High-level and low-level agents determine optimal actions under dynamic pricing and power stability constraints. In addition, an uncertainty-aware augmentation is designed to adaptively adjust decisions to handle uncertain EV departures.
- **Practical Effectiveness:** We evaluate *HUCA* through analysis of real-world datasets, incorporating simulated EV behaviors in scenarios with both certain and uncertain departure times. Results demonstrate that *HUCA* achieves the lowest electricity costs while maintaining competitive performance in fulfilling EV charging requirements, which shows its potential as an AI-driven solution for intelligent vehicle charging control.

2 Preliminaries

This section delineates the essential symbols and their definitions. We also introduce the general formulations of Markov decision process (MDP) and deep deterministic policy gradient (DDPG) related to reinforcement learning techniques.

2.1 Key Symbols and Definitions. Let $\mathcal{C} = \{c_1, c_2, \dots, c_N\}$ denote a set of charging piles (abbreviated as piles henceforth) located at the office building’s charging station. $\mathcal{V}_t = \{v_1, v_2, \dots, v_M\}$ specifies a set of EVs docking at piles at time slot t , where $M \leq N$. The charging capacity of the charging station is denoted as \mathcal{P}^{\max} (kW), which represents the maximum allowable charging power at the station ($\mathcal{P}^{\max} > 0$). In contrast, the maximum allowable discharging power is denoted as

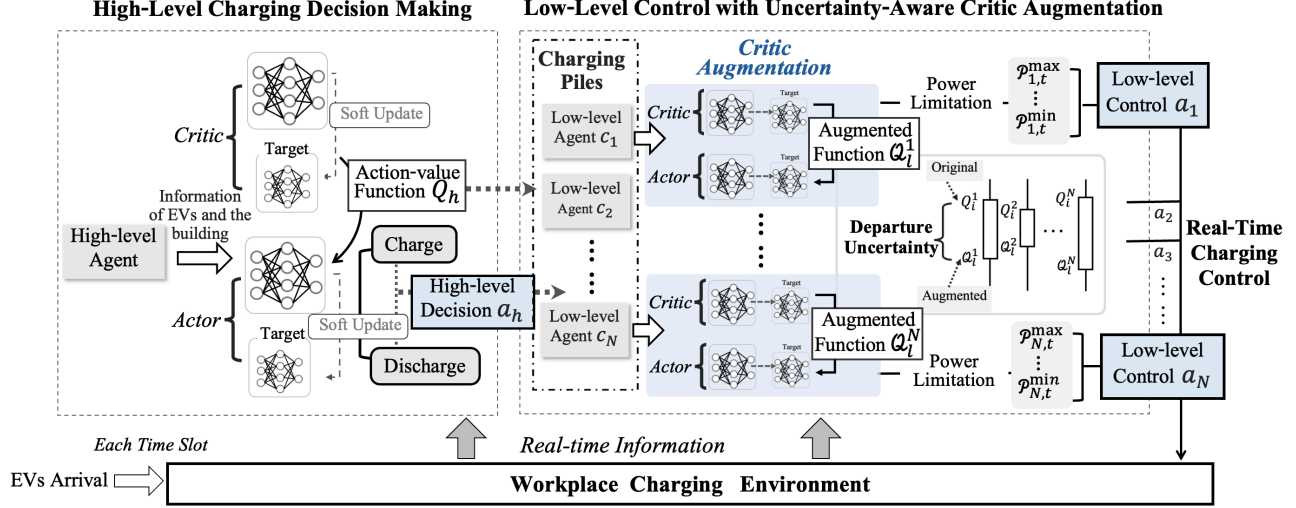


Figure 2: The overview of the HUCA framework. The high-level agent decides to charge or discharge EVs, while low-level agents control the power of each charging pile within power limitations.

$-\mathcal{P}^{\max}$ (kW).

Definition 1. (State of Charge (SoC)): The state of charge (SoC) of an EV battery represents the percentage of energy stored in the battery. For each EV $v_i \in \mathcal{V}_t$, the SoC of v_i at time slot t is denoted as $SoC_t^i \in [0\%, 100\%]$.

Definition 2. (EV Charging Information): In our scenario, when an EV arrives at the workplace charging system (Fig. 1) at time slot t and connects to pile c_i , the EV user sends the charging information \mathcal{I}^i to the charging system. The charging information is denoted as a tuple: $\mathcal{I}^i = (t_{\text{arr}}^i, t_{\text{dep}}^i, SoC_{\text{arr}}^i, SoC_{\text{dep}}^i, C^i)$, where t_{arr}^i and t_{dep}^i represent the arrival time and the *planned* departure time, respectively. SoC_{arr}^i and SoC_{dep}^i denote the SoC of the EV battery upon arrival and the *expected* SoC to be reached by the charging system before the departure time, respectively. C^i is the battery capacity of the EV. Note that in our scenario, the actual departure time of the EV user may randomly occur earlier than the planned time t_{dep}^i .

Definition 3. (Charging Power Limitation): To ensure power system stability, the charging power of each charging pile is limited by the maximum charging capacity \mathcal{P}^{\max} of the charging station. Given the number of EVs $|\mathcal{V}_t|$ docking at the charging station at time slot t , the maximum charging power P_t^{pile} of each pile at time slot t is estimated as $P_t^{\text{pile}} = \mathcal{P}^{\max}/|\mathcal{V}_t|$. The maximum discharging power of each pile is $-P_t^{\text{pile}}$.

To consider the fulfillment of the expected SoC SoC_{dep}^j of each EV v_j , we estimate the specific charging/discharging power boundary that pile c_i provides to the connected EV v_j at each time slot t , following the settings in [9, 11]. Specifically, given the minimum and maximum SoC that EV v_j can reach at time t , denoted

by SoC_t^{LB} and SoC_t^{UB} , respectively, the specific charging and discharging power boundaries of charging pile c_i are as follows:

$$\begin{cases} \mathcal{P}_{i,t}^{\max} = \min(P_t^{\text{pile}}, (SoC_t^{UB} - SoC_{t-1}^j \cdot C^i \cdot \eta^*)) \\ \mathcal{P}_{i,t}^{\min} = \max(-P_t^{\text{pile}}, (SoC_t^{LB} - SoC_{t-1}^j \cdot C^j \cdot \eta^*)) \end{cases},$$

where SoC_{t-1}^j is the SoC of v_j at time slot $t-1$, and C^j denotes the battery capacity for the EV. η^* is function of charging efficiency, as defined in [9, 11].

2.2 Markov Decision Process and Deep Deterministic Policy Gradient. Decision-making problems are commonly modeled as Markov decision processes (MDPs), which defined by the four-tuple information (S, A, R, T) : states S , actions A , rewards R and the state transition probabilities T . The main objective of an MDP is to find a policy that maximizes the cumulative rewards by selecting appropriate actions. The Deep Deterministic Policy Gradient (DDPG) algorithm [13], which is an actor-critic policy-based method that extends stochastic policy gradients to deterministic settings, has shown great effectiveness in complex environments. Specifically, its deep actor network, parameterized by θ^μ , approximates the deterministic policy $\mu_\theta : S \rightarrow A$. The critic network, parameterized by θ^Q , estimates the action-value function $Q(s, a|\theta^Q)$. Overall, the actor network determines the optimal action for a given state, while the critic network evaluates the action's quality.

2.3 Problem Formulation. Our work aims to benefit both the office building and EVs by enhancing the original single-agent DDPG framework. We model the

problem as a hierarchical MDP to optimize multiple objectives simultaneously, aiming to find the most effective bidirectional charging strategy that reduces building overall electricity costs while considering EV charging needs.

At each time slot t , given the charging pile set \mathcal{C} , EV set \mathcal{V}_t , EV charging information $\{\mathcal{I}^i|v_i \in \mathcal{V}_t\}$, and the charging and discharging power boundaries $\{\mathcal{P}_{i,t}^{\max}, \mathcal{P}_{i,t}^{\min}|v_i \in \mathcal{V}_t\}$, the objective is to determine the optimal charging (or discharging) power $\mathcal{P}_{i,t}^{\text{opt}}$ for each EV v_i at time slot t , where $\mathcal{P}_{i,t}^{\min} \leq \mathcal{P}_{i,t}^{\text{opt}} \leq \mathcal{P}_{i,t}^{\max}$. By determining $\mathcal{P}_{i,t}^{\text{opt}}$ in the certain departure scenario, where the EV's actual departure time matches the planned one, the goal is to minimize the total electricity cost of the building while ensuring that EV users' expected SoCs are met at their departure. In scenarios where EVs depart earlier than expected¹, our objective is to achieve their desired SoCs to the greatest extent while minimizing costs, balancing the trade-off between cost reduction and maximizing EV charging fulfillment.

3 The HUCA Framework

The architecture of HUCA is illustrated in Figure 2. Initially, a high-level agent determines whether to charge or discharge EVs using real-time data (Sec. 3.1). Subsequently, multiple low-level agents manage the charging and discharging power for each individual pile, taking into account the unpredictability of EV departures (Sec. 3.2). Finally, HUCA can determine the optimal decision instantaneously (Sec. 3.3).

3.1 High-Level Charging Decision Making.

This section formulates a novel MDP for a high-level agent to decide whether to charge or discharge EVs.

3.1.1 State representations. A state s_h , denoted by $s_h = (I_t^e, I_t^v, I_{t-1}^l)$, describes the status at the time slot t . The triplet includes: (i.) the electricity usage of the building and the electricity price, I_t^e ; (ii.) EVs situations, I_t^v ; and (iii.) the information learned by low-level agents at the previous time slot, I_{t-1}^l . Details are given in Appendix A.2.

3.1.2 Discrete actions for the high-level agent.

Let $a_h \in [0, 1]$ denote the action selected by the high-level agent. It is then converted into the discrete high-level action a_h^{disc} to determine whether to charge or discharge EVs, as defined below:

$$(3.1) \quad a_h^{\text{disc}} = \begin{cases} 1 & , \text{ if } a_h \geq 0.5 \\ 0 & , \text{ if } a_h < 0.5 \end{cases},$$

where $a_h^{\text{disc}} = 1$ represents charging, and $a_h^{\text{disc}} = 0$ denotes discharging.

3.1.3 High-level objective and reward function.

The total electricity cost of a building is calculated based on two parts: (i) the total electricity consumption and (ii) the amount of electricity exceeding the contracted capacity [7], which is the upper bound of instant electricity consumption. The objective of the high-level agent is to minimize the total electricity cost.

Let L_t represent the electricity load, ΔL_t denote the excess electricity consumption of the building, p_t be the electricity price, and t specify the time slot. The reward function $r_h(s_h, a_h^{\text{disc}})$, briefed as r_h , is defined as:

$$(3.2) \quad r_h = \kappa \cdot \underbrace{\left(- \sum_{t'=1}^t p_{t'} \cdot L_{t'} - \sum_{t'=1}^t \max(0, \Delta L_{t'}) \cdot \varphi \right)}_{\text{electricity cost term}} + \underbrace{\left(-|L_t - L_{\text{avg}}| \right)}_{\text{electricity balance term}},$$

where the first term represents the potential total electricity cost up to time t , weighted by an importance factor $\kappa \in [0, 1]$. $\varphi \in \mathbb{R}$ is a fixed penalty coefficient weighting the exceeding instant electricity usage. The second term balances the electricity consumption compared to the previous average load L_{avg} . This design reduces the reward for costly or imbalanced charging, encouraging the high-level agent to avoid similar actions in future comparable states.

To evaluate charging or discharging actions, we apply DDPG concepts to update the high-level policy μ_h . The high-level agent trains the critic network, with parameters θ_h^Q , to approximate action-value function $Q_h(s_h, a_h)$ by minimizing the following loss:

$$(3.3) \quad \mathcal{L}(\theta_h^Q) = \mathbb{E}_{s_h, a_h, r_h, s'_h \sim \mathcal{D}_h} \left[\left(Q_h(s_h, a_h) - y_h \right)^2 \right],$$

$$y_h = r_h + \gamma \bar{Q}_h(s'_h, a'_h) |_{a'_h = \mu_h(s'_h)},$$

where γ is a discount factor. \bar{Q}_h is the target Q-function used to stabilize learning. The replay buffer \mathcal{D}_h stores the transition experiences of the high-level agent in the form of tuples (s_h, a_h, r_h, s'_h) . Subsequently, the actor network θ_h^μ updates the high-level policy μ_h via gradient descent as follows:

¹When the departure occurs later than anticipated, achieving desired SoCs of these EVs is relatively straightforward compared to scenarios of early departure. Consequently, this paper concentrates on addressing the uncertainty of early departure.

(3.4)

$$\nabla_{\theta_h^\mu} J(\mu_h) = \mathbb{E}_{s_h, a_h \sim \mathcal{D}_h} \nabla_{\theta_h^\mu} \mu_h(a_h | s_h) \nabla_{a_h} Q_h(s_h, a_h) |_{a_h = \mu_h(s_h)}$$

3.2 Low-Level Control with Uncertainty-Aware Critic Augmentation.

Based on the charging or discharging decision made by the high-level action, the goal of the low-level control is to determine the optimal charging (or discharging) power level for each pile, taking into account the uncertainty of EV departures. Each pile $c_i \in \mathcal{C}$ is regarded as a low-level agent and its task is formulated as an MDP. A multi-agent structure including multiple piles is deployed for low-level control.

3.2.1 State representations. For a low-level agent $c_i \in \mathcal{C}$, the state s_t^i observed at time slot t comprises two information $s_t^i = (I_t^{v_j}, I_t^h)$: (i) the real-time charging information of the connected EV $v_j \in \mathcal{V}_t$, denoted as $I_t^{v_j}$; and (ii) the information learned by the high-level agents, denoted as I_t^h . For simplicity of the presentation, we provide additional details in Appendix A.2.

3.2.2 Low-level objective and the critic augmentation. Multi-agent DDPG (MADDPG) [14] extends DDPG into a multi-agent policy gradient algorithm, where decentralized agents learn a centralized critic based on the observations and actions of all agents. Inspired by MADDPG, we formulate the objective of each critic network, $\theta_h^{Q,i}$, of a low-level agent $c_i \in \mathcal{C}$ by minimizing the following loss:

$$(3.5) \quad \mathcal{L}(\theta_h^{Q,i}) = \mathbb{E}_{\mathbf{x}, \mathbf{a}, \mathbf{r}, \mathbf{x}' \sim \bigcup_{c_i \in \mathcal{C}} \{\mathcal{D}_i^i\}} \left[\left(Q_i^i(\mathbf{x}, a_1^1, \dots, a_1^N) - y_i^i \right)^2 \right],$$

$$y_i^i = r_i^i + \gamma \bar{Q}_i^i(\mathbf{x}', a_1^1, \dots, a_1^N) |_{a_1^j = \mu_1^j(s_1^j)},$$

where $\mathbf{x} = \{s_1^1, s_1^2, \dots, s_1^N\}$ collects the states of all low-level agents. \mathcal{D}_i^i is the replay buffer of agent c_i , storing the transition experience with tuples $(s_1^i, a_1^i, r_1^i, s_1^i)$. Q_i^i is the action-value function from the critic network of agent c_i , and \bar{Q}_i^i is the target Q-function.

However, early departures of EVs occur occasionally, making the departure time uncertain and complicating the selection of the best low-level actions. To tackle this challenge, inspired by the Upper Confidence Bound (UCB) algorithm [1], which adjusts action-value estimations based on uncertainty (or confidence) and thereby affects the action decision, we propose a novel *augmented action-value function*, \mathcal{Q}_i^i , for the **actor network** of each low-level agent c_i . The idea is to discourage higher power level discharging actions when the

given expected departure time is approaching and the expected SoC is still unmet. This augmentation incorporates uncertainty into the actor network for decision-making, while isolating direct impact of uncertainties from the critic network training, thereby maintaining the robustness of the critic network. Accordingly, \mathcal{Q}_i^i is designed as follows:

(3.6)

$$\mathcal{Q}_i^i(\mathbf{x}, \mathbf{a}) = Q_i^i(\mathbf{x}, a_1^1, \dots, a_1^N) \cdot \left(1 - \underbrace{\rho \cdot |\log_2(\bar{a}_1^i + \epsilon)| \cdot \sqrt{\frac{\max(\Delta SoC_t^i, 0)}{\Delta T_t^i}}}_{\text{the uncertainty factor}} \right),$$

where $\bar{a}_1^i \in [0, 1]$ is the action chosen by low-level agent c_i . A smaller \bar{a}_1^i indicates a tendency for higher discharge power, as defined in Sec. 3.2. ΔSoC_t^i represents the difference between the expected SoC SoC_{dep}^i and the current SoC SoC_t^i of the EV connected to pile c_i . ΔT_t^i is the time difference between the current time t and the planned departure time t_{dep}^i . $\rho \in \mathbb{R}$ is a fixed coefficient representing the impact of uncertainty, and ϵ is a small constant. Consequently, high power discharging action is penalized when the uncertainty factor increases.

Based on Eq. 3.6, the actor network $\theta_t^{\mu,i}$ of low-level agent c_i updates the low-level policy μ_t^i with gradient descent as follows:

(3.7)

$$\nabla_{\theta_t^{\mu,i}} J(\mu_t^i) = \mathbb{E}_{\mathbf{x}, \mathbf{a} \sim \bigcup_{c_i \in \mathcal{C}} \{\mathcal{D}_i^i\}} \left[\nabla_{\theta_t^{\mu,i}} \mu_t^i(a_1^i | s_1^i) \nabla_{a_1^i} \mathcal{Q}_i^i(\mathbf{x}, \mathbf{a}) |_{a_1^i = \mu_t^i(s_1^i)} \right].$$

3.2.3 Continuous actions and the reward function for low-level agents.

Let $a_1^i \in [0, 1]$ be the action selected by a low-level agent c_i . To entangle low-level action space with the high-level discrete decision a_h^{disc} , the continuous action \bar{a}_1^i is formulated as follows:

$$(3.8) \quad \bar{a}_1^i = \begin{cases} \delta + \delta \cdot \sigma(a_1^i) & , \text{ if } a_h^{\text{disc}} = 1 \\ \delta \cdot \sigma(a_1^i) & , \text{ if } a_h^{\text{disc}} = 0 \end{cases},$$

where $\sigma(\cdot)$ is the sigmoid function, and δ is set to 0.5. In this setting, the action space of a_1^i is constrained to $[0, 0.5)$ while the discrete high-level action is “discharging” ($a_h^{\text{disc}} = 0$). In contrast, a_1^i is limited to $[0.5, 1]$ when the high-level action is “charging” ($a_h^{\text{disc}} = 1$).

Subsequently, the optimal charging/discharging power $\mathcal{P}_{i,t}^{\text{opt}}$ provided by low-level agent (pile) $c_i \in \mathcal{C}$ to the connected EV at time slot t is estimated based

on the continuous low-level action a_l^i , as defined below:

$$(3.9) \quad \mathcal{P}_{i,t}^{\text{opt}} = \bar{a}_l^i \cdot (\mathcal{P}_{i,t}^{\text{max}} - \mathcal{P}_{i,t}^{\text{min}}) + \mathcal{P}_{i,t}^{\text{min}}.$$

Based on the selected action a_l^i and the optimal power decision $\mathcal{P}_{i,t}^{\text{opt}}$ at each time slot, the reward function $r_l(s_l^i, a_l^i)$ (abbreviated as r_l^i) for the low-level agent (pile) c_i is formulated based on the charging cost at the current time slot t and the difference between the current SoC and the expected SoC at the EV’s departure connected to c_i , defined as follows:

$$(3.10) \quad r_l = \omega \cdot (-\mathcal{P}_{i,t}^{\text{opt}} \cdot p_t) + (-|SoC_t^i - SoC_{\text{dep}}^i|),$$

where p_t and SoC_t^i are the energy price and the SoC of the EV at time slot t , respectively. SoC_{dep}^i is the expected SoC at the EV’s departure. The parameter ω reflects the impact of the current charging cost.

3.3 Optimization for the Hierarchical Control.

Based on Sec. 3.1 and Sec. 3.2, the critic and actor networks are optimized with minibatches of samples from the replay buffers, which follows the soft update rule. Let $\theta_h = \{\theta_h^Q, \theta_h^\mu\}$ and $\theta_l^i = \{\theta_l^{Q,i}, \theta_l^{\mu,i}\}$ represent the parameters of target critic and actor networks of the high-level agent and the low-level agent (c_i), respectively. The parameters updates are as follows:

$$(3.11) \quad \theta_h' \leftarrow \tau \theta_h + (1 - \tau) \theta_h', \quad \theta_l^{i'} \leftarrow \tau \theta_l^i + (1 - \tau) \theta_l^{i'},$$

where $\tau \in [0, 1]$ is the coefficient controlling the update rate. Through these optimizations, the decision-making processes of both high-level and low-level agents are refined without requiring future information. The details of optimization formulation are given in Appendix A.3.

4 Experimental Results

4.1 Dataset and Experimental Setup.

4.1.1 Dataset Description and Preprocessing.

For our workplace charging system scenario, we use the following datasets: (i) Building electricity demands: the CU-BEMS dataset [17] provides office building electricity consumption. (ii) Pricing mechanism: the ComEd APIs [5] supply real-time pricing data. Also, the penalty mechanism is designed based on [18]. The data is aggregated into hourly intervals. The training period is from July 1, 2018, to August 31, 2018, with testing in the following month. Details are in Appendix A.1.

4.1.2 Simulation of EV Behaviors. The charging information $\mathcal{I}^i = (t_{\text{arr}}^i, t_{\text{dep}}^i, SoC_{\text{arr}}^i, SoC_{\text{dep}}^i, C^i)$ (Def.

2) of the EV is modeled using truncated normal distributions by following [10]. Table 1 shows the setting of random variables and C^i is set to 60 kWh. Two departure scenarios are examined:

- Certain departure scenario:** The actual departure time \hat{t}_{dep}^i is the same as the expected time t_{dep}^i .
- Uncertain departure scenario:** The actual departure time is randomly sampled earlier than the expected time, $\hat{t}_{\text{dep}}^i \in [1, t_{\text{dep}}^i)$.

Table 1: Random variables for EV information.

Information	Distribution	Boundaries
Arrival time	$\mathcal{N}(9, 1^2)$	$7 \leq t_{\text{arr}}^i \leq 12$
Expected departure time	$\mathcal{N}(19, 1^2)$	$16 \leq t_{\text{dep}}^i \leq 23$
SoC upon arrival	$\mathcal{N}(0.4, 0.1^2)$	$0.3 \leq SoC_{\text{arr}}^i \leq 0.6$
Expected SoC at departure	$\mathcal{N}(0.8, 0.1^2)$	$0.6 \leq SoC_{\text{dep}}^i \leq 0.9$

4.1.3 Baselines.

We compare our *HUCA* with following baselines. **OPT**: An oracle with full knowledge of future information serves the optimal solution of minimal total cost and minimal penalty cost. We include the single-agent (**DDPG** [9]) and multi-agent reinforcement learning models (**IQL** [23], **VDN** [22], and **MADDPG** [21]). These details are provided in Appendix A.1.4.

4.1.4 Evaluation Metrics.

- Penalty Cost (USD)** measures the cost of exceeding the contracted capacity [7], which multiplies the penalty rate with the peak amount of electricity (check Appendix A.1 for details).
- Total Cost (USD)** is the sum of the basic electricity cost (electricity load L_t multiplied by dynamic pricing p_t) and the penalty cost over the testing data.

In the **certain departure scenario**, *all EV charging demands are met* since all baselines are subject to the charging power limitations (Sec. 2.1, Def. 3) and no unexpected EV departures occur. In the **uncertain departure scenario**, how well the charging demands are fulfilled when unexpected EV departures happen needs examinations. Given $\widehat{SoC}_{\text{dep}}^i$ and SoC_{dep}^i denoting the actual and expected SoC of EV v_i at the time of departure, and SoC_{arr}^i is the SoC of v_i upon arrival at the parking lot, the metrics are defined as follows:

- SoC Fulfillment (%)** evaluates how well the expected SoC of EV v_i is fulfilled, defined as: $\widehat{SoC}_{\text{dep}}^i / SoC_{\text{dep}}^i$.

Table 2: Performance comparison (*HUCA* performance) with different number of charging piles (CP). Except of the “OPT” method, the best and second best results for “Penalty Cost” (↓) and “Total Cost” (↓) are in **bold** and underlined, respectively. Cells in gray highlight the results that are greater than or equal to the median value for “SoC Maintenance” (↑), “SoC Fulfillment” (↑) and “User Satisfaction” (↑).

Certain Departure Scenario	Metric	CP	OPT	DDPG	IQL	VDN	MADDPG	<i>HUCA</i>
	Penalty Cost (USD)	10	0.00	3682.85	2516.84	522.28	<u>354.84</u>	354.82
Total Cost (USD)	5805.28		9563.31	8426.36	6431.31	<u>6220.33</u>	6215.42	
Penalty Cost (USD)	20	0.00	7818.52	5643.15	2271.32	<u>1869.38</u>	1643.47	
Total Cost (USD)		5860.05	13929.11	11798.68	8413.61	<u>7952.69</u>	7728.57	

Uncertain Departure Scenario	Metric	CP	OPT	DDPG	IQL	VDN	MADDPG	<i>HUCA</i>
	Penalty Cost (USD)	10	0.00	4671.74	1742.35	529.18	<u>448.52</u>	355.84
Total Cost (USD)	5691.96		10398.77	7479.04	6214.53	<u>6087.48</u>	5993.78	
SoC Fulfillment (%)			53.77	54.05	46.04	40.34	27.10	40.77
SoC Maintenance (%)			42.52	-10.58	129.01	-120.61	<u>11.87</u>	45.40
User Satisfaction (%)			48.14	21.73	87.52	-40.13	19.48	43.08
Penalty Cost (USD)	20	0.00	5010.81	2002.12	966.51	<u>931.01</u>	354.90	
Total Cost (USD)		5760.05	10823.07	7815.99	6721.82	<u>6562.80</u>	6013.52	
SoC Fulfillment (%)			56.06	55.27	47.94	48.88	40.34	42.44
SoC Maintenance (%)			32.77	12.56	0.90	91.96	-1.16	124.41
User Satisfaction (%)			44.41	33.91	24.42	70.42	19.59	83.42

Table 3: Ablation study results for the uncertain departure scenario. (SoC fulfillment and maintenance scores are abbreviated as “Ful.” and “Main.”, respectively.)

CP	Method	Penalty ↓	Total ↓	Ful. ↑	Main. ↑
10	<i>HUCA</i>	355.84	5993.78	40.77 %	45.40%
	w/o C.A.	2015.62	7761.55	62.49%	124.01%
	w/o H.	2707.71	8483.96	63.10%	31.91%
	w/o Either	723.46	6393.26	44.53%	-12.53%
20	<i>HUCA</i>	354.90	6013.52	42.44%	124.41%
	w/o C.A.	9362.87	15309.23	69.73%	209.70%
	w/o H.	3461.37	9261.72	58.61%	7.69%
	w/o Either	618.46	6381.87	53.26%	43.02%

- **SoC Maintenance (%)** checks the fulfillment status at the midpoint (\widehat{SoC}_{mid}^i) between the arrival and the actual departure time, verifying whether the SoC is consistently maintained under the charging control. A drop below the arrival SoC would result in extra expenses billed to users. The metric is defined as: $(\widehat{SoC}_{mid}^i - SoC_{arr}^i) / (\widehat{SoC}_{dep}^i - SoC_{arr}^i)$, where \widehat{SoC}_{mid}^i denotes the SoC at the midpoint.
- **User Satisfaction (%)** represents the average of SoC fulfillment and SoC maintenance, indicating EV users’ satisfaction with the charging performance.

The performance of these three metrics is reported as the average for all EVs per parking session.

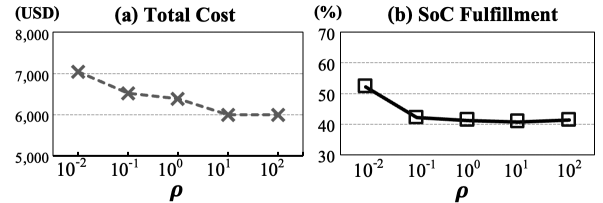


Figure 3: Performance of *HUCA* with different ρ values with 10 piles in the uncertain departure scenario.

4.2 Comparison Results. As shown in Table 2, except for the “OPT” method (best-case result), *HUCA* achieves the lowest penalty and total costs that do not rely on future information for charging control across both departure scenarios. In addition, its total cost is comparable to OPT, manifesting its effectiveness in minimizing costs. Although the SoC fulfillment, maintenance, and user satisfaction scores of *HUCA* are not the best, it still achieves a comparable results to all the other baselines. Note that combining the above observations, *HUCA* actually strikes the best balance between the trade-off of electricity costs and fulfilling user demands by introducing the hierarchical control and the uncertainty-aware critic augmentation.

Among the multi-agent models, VDN and MADDPG come closest to *HUCA* in terms of cost. However, the user satisfaction scores of MADDPG are much lower than those of *HUCA* across different numbers of charging piles. While VDN achieves higher SoC fulfillment score than *HUCA* with 20 charging piles, its mainte-

nance scores are significantly lower. With 10 charging piles, VDN’s maintenance score even drops to a negative value (-120.61%), indicating that under MADDPG and VDN control, EVs’ SoCs are not maintained at arrival levels. Therefore, EVs primarily serve as power providers rather than being effectively charged, resulting in additional expenses for users.

4.3 Ablation Study and Analysis of the Uncertainty Impact. We conduct an ablation study by removing the uncertainty-aware critic augmentation (**w/o C.A.**), the high-level agent (**w/o H.**), and both of them (**w/o Either**). The results are shown in Table 3. Compared to *HUCA*, removing either the critic augmentation or the high-level agent increases SoC fulfillment and maintenance scores. However, this also leads to a significant rise in both penalty and total costs. On the other hand, removing both components results in a slight increase in costs but causes a significant drop in SoC maintenance scores. These findings indicate that the hierarchical structure and critic augmentation in *HUCA* complement each other, and their combined use is essential for achieving the lowest costs while effectively balancing energy supply between the office building and EVs.

Furthermore, to assess the impact of the uncertainty term in *HUCA* for handling uncertain departures, Figure 3 compares total cost and the SoC fulfillment under various uncertainty coefficient ρ (Eq. 3.6). As ρ increases, total cost decreases significantly. Meanwhile, setting ρ to its lowest value (10^{-2}) improves SoC fulfillment but comes at the cost of significantly higher total costs. These findings suggest that ρ should not be set too low to ensure a better trade-off between cost and user charging demand. Properly tuning ρ can further improve this balance, enhancing the overall effectiveness of *HUCA*.

4.4 Case Study. To examine how *HUCA* balances energy supply between the building and EVs, Figure 4 visualizes the control decisions over a day. Two significant EV charging behaviors appear at 7:00 and 16:00 (red rectangle). At 7:00, both electricity demand and prices for the building are minimal (Figure 4(a)), therefore *HUCA* focuses on charging the EVs to reach their target SoC. At 16:00, even though there is a high demand for building energy and elevated prices, which typically would lead to transferring energy from the EVs to the building to reduce costs, *HUCA* opts to charge the EVs because of their high charging urgency (Figure 4(b)) using Eq. (3.6). In contrast, at 8:00 (green rectangle), *HUCA* discharges EVs to serve the high-usage building and avoid high pricing time simultaneously. These results manifest that *HUCA* effectively and dynamically

balances energy supply between the building and EVs based on real-time information.

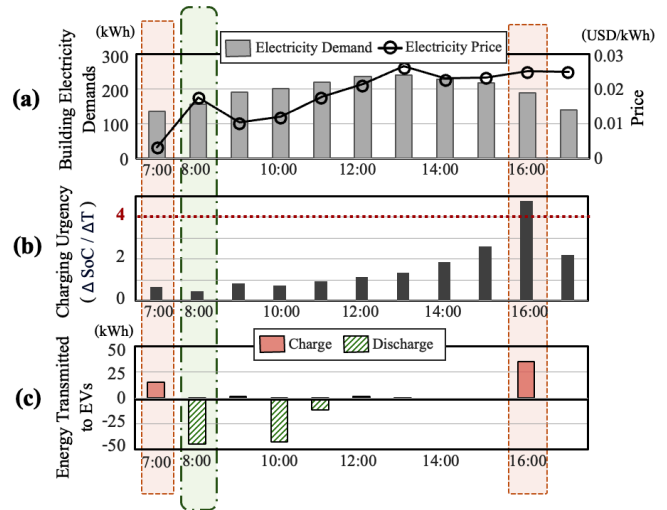


Figure 4: Details of the charging control for a day from 7:00 to 17:00. (a) shows building electricity demands and dynamic pricing; (b) visualizes average charging urgency, with ΔSoC as the difference between current and expected SoC, and ΔT as the remaining time until planned departure; (c) presents final control decisions.

5 Related Work

5.1 Real-time Charging Control. Guo *et al.* [8] combined day-ahead optimization with real-time control to address uncertainties in solar output and EV parking behaviors. Chandra Mouli *et al.* [16] introduced an energy management system with vehicle-to-grid (V2G) services to adjust charging control. Chopra *et al.* [3] conducted a cost-benefit analysis for EV charging infrastructure in parking lots. Zhao *et al.* [30] employed risk-based day-ahead scheduling for EV aggregators using information gap decision theory to minimize building costs. Zhang *et al.* [29] developed an EV load optimization model to reduce grid-level energy costs by considering peak and valley electricity prices. Chen *et al.* [2] devised strategies for battery energy storage systems to participate in peak load shifting, minimizing load fluctuations.

5.2 Reinforcement Learning for Charging Management. Single-agent RL, multi-agent RL (MARL), and hierarchical MARL approaches were used to manage charging systems. Single-agent RL represented the control system [12, 15] under various considerations, such as ensuring EV battery requirements [27] and addressing charger shortage [9]. MARL modeled fine-grained cooperations [26] among EVs and buildings to

tackle safety concerns [28] and power transfer overload [6]. Hierarchical MARL further separated system operators and EV users, and coordinated them to minimize demand charges and energy costs [20].

Although literature in Sec. 5.1 and 5.2 optimized charging control with various aspects, most studies do not address the issue of uncertain EV departures. While some works [8, 15, 28] considered uncertainties in EV behavior, they primarily focused on a single objective, such as maximizing system revenue or minimizing user charging costs. In contrast, our work tackles dynamic factors, including fluctuating electricity prices and uncertain EV departures, aiming to simultaneously minimize total electricity costs for the charging system while accounting for EV users' charging demands.

6 Conclusion

In this paper, we propose *HUCA*, a novel hierarchical multi-agent framework designed for real-time charging control in the workplace charging scenario. To address practical dynamics and limitations, *HUCA* integrates a hierarchical control and uncertainty-aware critic augmentation. With this design, *HUCA* adapts to dynamic factors, optimizes charging or discharging power for each charging pile, and accounts for departure uncertainties in evaluating the quality of charging control. Experiments demonstrate that, in both certain and uncertain departure scenarios, *HUCA* outperforms existing methods by achieving the lowest electricity costs while maintaining competitive performance in meeting EV charging requirements. A case study further illustrates that *HUCA* effectively balances energy supply between the building and EVs using real-time information.

References

- [1] P Auer. Finite-time analysis of the multiarmed bandit problem, 2002.
- [2] Yutian Chen, Xiuli Wang, Jianxue Wang, Tao Qian, and Qiao Peng. Power control strategy of battery energy storage system participating in power system peak load shifting. *2020 5th Asia Conference on Power and Electrical Engineering (ACPEE)*, pages 710–715, 2020.
- [3] Krishan Chopra, Mukesh kumar Shah, and Khaleequr Rehman Niazi. Cost benefit analysis for electric vehicle charging infrastructure in parking lot. *2023 IEEE IAS Global Conference on Renewable Energy and Hydrogen Technologies (GlobConHT)*, pages 1–5, 2023.
- [4] Coldwell Banker Richard Ellis Group Inc. EV adoption creates more demand for workplace charging stations, 2024.
- [5] ComEd. Comed hourly pricing, 2024. Accessed: 2024-07-18.
- [6] Felipe Leno da Silva, Cyntia Eico Hayama Nishida, Diederik M. Roijers, and Anna Helena Reali Costa. Coordination of electric vehicle charging through multiagent reinforcement learning. *IEEE Transactions on Smart Grid*, 11:2347–2356, 2020.
- [7] Miguel A. Fernández, Angel L. Zorita, Luis Angel García-Escudero, Oscar Duque, D. Morinigo, M. V. Risco, and M. G. Muñoz. Cost optimization of electrical contracted capacity for large customers. *International Journal of Electrical Power & Energy Systems*, 46:123–131, 2013.
- [8] Yi Guo, Jingwei Xiong, Shengyao Xu, and Wencong Su. Two-stage economic operation of microgrid-like electric vehicle parking deck. *IEEE Transactions on Smart Grid*, 7:1703–1712, 2016.
- [9] Hang Li, Guojie Li, Shidan Li, Bei Han, Keyou Wang, and Jin Xu. Optimal ev charging scheduling considering the lack of charging facilities based on deep reinforcement learning. *2023 8th Asia Conference on Power and Electrical Engineering (ACPEE)*, pages 1825–1829, 2023.
- [10] Hang Li, Guojie Li, Tek Tjing Lie, Xingzhi Li, Keyou Wang, Bei Han, and Jin Xu. Constrained large-scale real-time ev scheduling based on recurrent deep reinforcement learning. *International Journal of Electrical Power & Energy Systems*.
- [11] Hang Li, Guojie Li, Tek Tjing Lie, Xingzhi Li, Keyou Wang, Bei Han, and Jin Xu. Constrained large-scale real-time ev scheduling based on recurrent deep reinforcement learning. *International Journal of Electrical Power and Energy Systems*, 144:108603, 2023.
- [12] Hepeng Li, Zhiqiang Wan, and Haibo He. Constrained ev charging scheduling based on safe deep reinforcement learning. *IEEE Transactions on Smart Grid*, 11:2427–2439, 2020.
- [13] Timothy P Lillicrap, Jonathan J Hunt, Alexander Pritzel, Nicolas Heess, Tom Erez, Yuval Tassa, David Silver, and Daan Wierstra. Continuous control with deep reinforcement learning. In *Proceedings of the 4th International Conference on Learning Representations (ICLR)*, 2016.
- [14] Ryan Lowe, Aviv Tamar, Jean Harb, OpenAI Pieter Abbeel, and Igor Mordatch. Multi-agent actor-critic for mixed cooperative-competitive environments. *Advances in neural information processing systems*, 30, 2017.
- [15] Naram Mhaisen, Noora Fetais, and Ahmed Mohammed Massoud. Real-time scheduling for electric vehicles charging/discharging using reinforcement learning. *2020 IEEE International Conference on Informatics, IoT, and Enabling Technologies (ICIoT)*, pages 1–6, 2020.
- [16] Gautham Ram Chandra Mouli, Mahdi Kefayati, Ross Baldick, and Pavol Bauer. Integrated pv charging of ev fleet based on energy prices, v2g, and offer of reserves. *IEEE Transactions on Smart Grid*, 10:1313–

- 1325, 2019.
- [17] M. Pipattanasomporn, G. Chitalia, J. Songsiri, and et al. Cu-bems, smart building electricity consumption and indoor environmental sensor datasets. *Sci Data*, 7:241, 2020.
- [18] Barbara Rosado, Ricardo Torquato, Bala Venkatesh, Hoay Beng Gooi, Walimir Freitas, and Marcos J Rider. Framework for optimizing the demand contracted by large customers. *IET Generation, Transmission & Distribution*, 14(4):635–644, 2020.
- [19] I Sami, Z Ullah, K Salman, I Hussain, SM Ali, B Khan, CA Mehmood, and U Farid. A bidirectional interactive electric vehicles operation modes: Vehicle-to-grid (v2g) and grid-to-vehicle (g2v) variations within smart grid. In *2019 international conference on engineering and emerging technologies (ICEET)*, pages 1–6. IEEE, 2019.
- [20] Can Berk Saner, Anupam Trivedi, and Dipti Srinivasan. A cooperative hierarchical multi-agent system for ev charging scheduling in presence of multiple charging stations. *IEEE Transactions on Smart Grid*, 13(3):2218–2233, 2022.
- [21] Amin Shojaeighadikolaei and Morteza Hashemi. An efficient distributed multi-agent reinforcement learning for ev charging network control. *2023 59th Annual Allerton Conference on Communication, Control, and Computing (Allerton)*, pages 1–8, 2023.
- [22] Peter Sunehag, Guy Lever, Audrunas Gruslys, Wojciech Marian Czarnecki, Vinicius Zambaldi, Max Jaderberg, Marc Lanctot, Nicolas Sonnerat, Joel Z Leibo, Karl Tuyls, et al. Value-decomposition networks for cooperative multi-agent learning based on team reward. In *Proceedings of the 17th International Conference on Autonomous Agents and MultiAgent Systems*, pages 2085–2087, 2018.
- [23] Ardi Tampuu, Tabet Matiisen, Dorian Kodelja, Ilya Kuzovkin, Kristjan Korjus, Juhan Aru, Jaan Aru, and Raul Vicente. Multiagent cooperation and competition with deep reinforcement learning. *PLoS ONE*, 12, 2015.
- [24] Rajendra Prasad Upputuri and Bidyadhar Subudhi. A comprehensive review and performance evaluation of bidirectional charger topologies for v2g/g2v operations in ev applications. *IEEE Transactions on Transportation Electrification*, 10(1):583–595, 2023.
- [25] Arjun Visakh and Manickavasagam Parvathy Selvan. Analysis and mitigation of the impact of electric vehicle charging on service disruption of distribution transformers. *Sustainable Energy, Grids and Networks*, 35:101096, 2023.
- [26] Linfang Yan, Xia Chen, Yin Chen, and Jinyu Wen. A cooperative charging control strategy for electric vehicles based on multiagent deep reinforcement learning. *IEEE Transactions on Industrial Informatics*, 18:8765–8775, 2022.
- [27] Feiye Zhang, Qingyu Yang, and Dou An. Cddpg: A deep-reinforcement-learning-based approach for electric vehicle charging control. *IEEE Internet of Things Journal*, 8:3075–3087, 2021.
- [28] Jin Zhang, Yuxiang Guan, Liang Che, and Mohammad Shahidehpour. Ev charging command fast allocation approach based on deep reinforcement learning with safety modules. *IEEE Transactions on Smart Grid*, 15:757–769, 2024.
- [29] Zhiying Zhang, Wenyi Li, and Xiaolong Li. Electric vehicle load optimization model considering peak and valley electricity price time. *2023 IEEE 2nd International Conference on Electrical Engineering, Big Data and Algorithms (EEBDA)*, pages 54–58, 2023.
- [30] Jian Zhao, Can Wan, Zhao Xu, and Jianhui Wang. Risk-based day-ahead scheduling of electric vehicle aggregator using information gap decision theory. *IEEE Transactions on Smart Grid*, 8:1609–1618, 2017.

A Reproducibility

A.1 Detailed Experimental Settings.

A.1.1 Dataset Preprocessing. We utilize the CU-BEMS dataset [17], which contains detailed energy consumption data from an office building, recorded at one-minute intervals from July 2018 to December 2019. For dynamic pricing (real-time pricing) data, we use the APIs [5] provided by ComEd (Commonwealth Edison), an electric utility company, offering real-time 5-minute electricity pricing data through its hourly pricing program. In our study, we aggregate the total energy consumption from all electrical appliances in the CU-BEMS dataset into hourly data to represent the building’s energy consumption in our workplace charging scenario. The dynamic pricing data obtained from ComEd APIs is similarly aggregated into hourly intervals. The training period covers July 1, 2018, to August 31, 2018, and the testing period runs from September 1, 2018, to September 30, 2018.

A.1.2 Penalty Mechanism. For the design of the penalty mechanism, the penalty charge is typically two or three times the basic capacity rate [18]. We design the penalty system based on the amount of electricity exceeding the contracted capacity (the upper bound of instant electricity consumption) [7, 18], with detailed settings shown in Table 4. Let the maximum instant electricity load during the testing period be L_{max} . If $L_{max} < C_{contract}$, then the penalty is set to zero. Given a threshold coefficient $0 < \delta < 1$, the penalty is calculated by dividing the excess electricity into two tiers:

1. Tier 1 (Up to 10% Overload): For overloads up to 10% of the contract capacity ($0 < L_{max} \leq \delta \cdot C_{contract}$), the penalty charge is set to $2 \cdot R_{base}$.
2. Tier 2 (Beyond 10% Overload): For overloads ex-

ceeding 10% of the contracted capacity ($L_{max} > \delta \cdot C_{contract}$), the penalty charge is set to $3 \cdot R_{base}$ for the amount that surpasses the 10% threshold.

Table 4: Design of the penalty mechanism.

Parameter	Value
Contract Capacity ($C_{contract}$)	700 kW
Basic Capacity Rate (R_{base})	\$15/kW/month
Exceed Electricity Amount	Penalty Charge
Up to 10% over $C_{contract}$	$2 \cdot R_{base}$
More than 10% over $C_{contract}$	$3 \cdot R_{base}$

Based on this setting, the total penalty cost is estimated as follows:

$$(A.1) \quad \text{Penalty Cost} = 2 \cdot R_{base} \cdot \min(L_{max}, \delta \cdot C_{contract}) + 3 \cdot R_{base} \cdot \max(0, L_{max} - \delta \cdot C_{contract}).$$

A.1.3 Hyperparameter Settings. The charging capacity (\mathcal{P}^{\max}) is set to 150 (kW), the EV battery capacity C^i (Def. 2) is 60 (kwh), and the charging efficiency is 95%. For training our *HUCA* model, we use 1,500 episodes, with a replay buffer capacity of 30,000 for each low-level agent, and a batch size of 1,024. The penalty coefficient φ (Eq. 3.2) weight factors κ (Eq. 3.2), ω (Eq. 3.10), and the importance of the uncertainty term ρ (Eq. 3.6) are set to 0.1, 0.1, 0.5, and 10, respectively.

A.1.4 Baseline Settings. To evaluate the performance of the proposed *HUCA* model, we compared it against several established baseline approaches:

- **OPT:** Assumes complete knowledge of future information, including all EV charging schedules, building energy demands, and dynamic electricity prices. This baseline uses a linear programming optimization model to solve the charging control problem.
- **DDPG (Deep Deterministic Policy Gradient)** [9]: An actor-critic algorithm designed for continuous control in single-agent environments.
- **IQL (Independent Q-Learning)** [23]: A decentralized multi-agent reinforcement learning approach where each agent independently learns its own Q-function.
- **VDN (Value Decomposition Networks)** [22]: A centralized value-based reinforcement learning method used in multi-agent systems.

- **MADDPG (Multi-Agent Deep Deterministic Policy Gradient)** [21]: Extends DDPG to multi-agent settings by incorporating centralized training and decentralized execution.

Note that for all models (except for OPT), the states, actions, and rewards are configured in the same manner as for our low-level agents, but without incorporating the information provided by the high-level agent network.

A.2 State representations of high-level and low-level MDPs.

A.2.1 High-level Agent. A state s_h in the MDP optimized by the high-level agent includes three main information $s_h = (I_t^e, I_t^v, I_{t-1}^l)$ at current time slot t . The details are as follows:

- I_t^e includes the electricity load of the building and electricity price for the following periods: the current time slot, the average over the past n hours, and the historical price at the same time and day of the week.
- I_t^v includes the current number of EVs at the charging station and the amount of energy provided to them.
- I_{t-1}^l includes the average critic value (from the action-value function) and the standard deviation of all low-level agents from the previous time slot.

A.2.2 Low-level Agent. For a low-level agent $c_i \in \mathcal{C}$, the state s_i^l observed at time slot t can be described as comprising two main information $s_i^l = (I_t^{v_j}, I_t^h)$. Details are:

- $I_t^{v_j}$ includes the current SoC of EV v_j and the suitable maximum and minimum charging powers ($\mathcal{P}_{i,t}^{\max}$ and $\mathcal{P}_{i,t}^{\min}$) of agent (charging pile) c_i as defined in Eq. 2.1.
- I_t^h includes the discrete high-level action a_h^{disc} determined at time slot t , and the critic value of state-action pair (s_h, a_h) obtained from the high-level critic network $Q_h(s_h, a_h; \theta_h^Q)$ at time slot t .

A.3 Optimization of *HUCA*. We optimize the *HUCA* framework using minibatches of samples from the replay buffers. For the high-level agent, given a minibatch of \mathcal{M} samples from the replay buffer \mathcal{D}_h , the training loss of the critic network is rewritten as:

$$(A.2) \quad \mathcal{L}(\theta_h^Q) = \frac{1}{\mathcal{M}} \sum_m \left(Q_h(s_h^m, a_h^m) - y_h^m \right)^2.$$

The actor network is updated using the sampled policy gradient as:

$$(A.3) \quad \nabla_{\theta_h^\mu} J(\mu_h) \approx \frac{1}{\mathcal{M}} \sum_m \nabla_{\theta_h^\mu} \mu_h(a_h^m | s_h^m) \nabla_{a_h} Q_h(s_h^m, a_h^m).$$

Similarly, the critic and actor networks of each low-level agent c_i are also optimized using minibatches.

B Limitation and Future Work

Despite the strong performance of *HUCA* and its consideration of multiple dynamic factors, we have not yet accounted for user willingness to adjust their charging preferences to supply energy to the building. A promising direction for future work is to incorporate user willingness, along with the buy-and-sell energy behaviors between users and the system, into our operational framework. User willingness could be integrated into the low-level actor-critic networks of *HUCA*. In our current design, the departure uncertainty term is used to set a lower confidence bound for the action-value function of each low-level agent. When incorporating user willingness, an incentive mechanism could be developed to estimate the upper confidence bound of the action-value function, as user willingness and incentives might increase the effectiveness of charging control.

This would not only help identify which EV users have greater flexibility in participating in energy control but also allow the system to evaluate both the lower and upper bounds of the potential quality of low-level actions. This approach could improve the optimal charging and discharging power control, enhancing both user satisfaction and the overall effectiveness of the system.